2026 IEEE International Conference on Robotics and Automation (ICRA 2026)
June 1-5, 2026. Vienna, Austria

Design and Implementation of an Angle-Bisecting Foot Mechanism for a Leg-Wheel Transformable Robot

Hsing-Chen Lee, Wei-Shun Yu, and Pei-Chun Lin*, *Senior Member, IEEE*

***Abstract*—This paper presents the design, modeling, and experimental validation of a novel leg-wheel mechanism featuring an integrated, passive angle-bisecting foot. The core of the design is a two-stage planetary gear system. This system mechanically ensures a consistent foot-ground contact angle, addressing a key limitation in transformable robots with symmetrical leg-wheels. To leverage this innovation, we developed a comprehensive kinematic model. Furthermore, we designed a hierarchical motion planning framework that utilizes the pure rolling motion enabled by the mechanism. The effectiveness of the proposed design was validated through hardware experiments on a 23 kg prototype. The results demonstrated improved energy efficiency based on the Cost of Transport (C.O.T.) metric, achieving up to a 16.2% reduction in C.O.T. alongside a 28.6% reduction in pitch oscillation compared to a baseline design. This study provides a valuable guideline for developing adaptive gait controllers that can optimize for energy efficiency in real time.**

***Index Terms*—Leg-wheel Robot, Hybrid Locomotion, Mechanism Design, Planetary Gears, Energy Efficiency, Legged Robot.**

I. Introduction

The demand for mobile robots capable of navigating complex, unstructured environments has driven significant advancements in legged locomotion. While dynamic quadruped robots such as MIT Cheetah [1], Spot [2] and HyQ [3] have demonstrated impressive agility in challenging terrains, a key challenge remains in balancing high mobility with energy efficiency. This has motivated the development of hybrid locomotion systems that seek to combine the respective advantages of different modalities.

The fusion of legs and wheels has emerged as a particularly promising approach, creating leg-wheel robots that leverage the energy efficiency of rolling on flat surfaces while retaining the obstacle-negotiation capabilities of legs. This paradigm has been explored through various platforms, such as ANYmal [4], MAX [5], RHex-T3 [6], and TerraAdapt [7]. The underlying leg kinematics for such systems often draw from advancements in both serial-chain and closed-loop linkage mechanisms, with designs like the Stanford Doggo [8], LDR [9] and other works [10]–[13] demonstrating the potential for lightweight and agile performance. This work is an evolution of a reconfigurable leg-wheel robot presented in [14]–[16], as part of an ongoing effort to create versatile robots capable of adapting their morphology for enhanced mobility across diverse terrains.

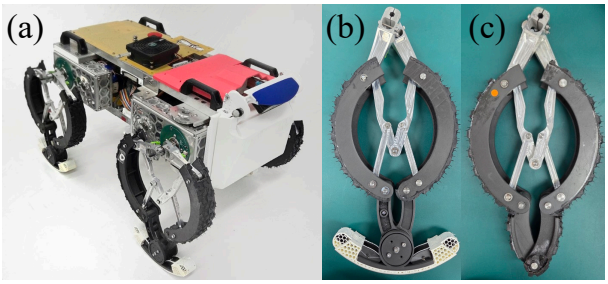

Fig. 1: Photo of the robot used in this research. (a): The robot used in this research. (b):The proposed design with angle-bisecting mechanism. (c): The baseline leg model

Despite these advancements in hybrid locomotion strategies, the critical interface between the robot and the environment—the foot—often remains a simplified component. While some research has focused on biomimetic foot and ankle designs to improve terrain adaptation and shock absorption [17]–[19], many transformable leg-wheel systems overlook the dynamic changes in foot posture during actuation. Specifically, for leg-wheel based on a symmetrical deployment mechanism, the foot's contact angle with the ground can vary significantly as the leg transforms. This variation compromises the stability of the ground contact, increasing the risk of slippage and reducing overall locomotor performance, especially on uneven or inclined surfaces. To address this critical gap, this paper introduces a novel leg-wheel design (shown in Fig. 1) featuring an integrated, passive angle-bisecting mechanism within the foot structure.

The main contributions of this work are as follows:

- The design of a novel leg-wheel mechanism that incorporates a planetary gear system to maintain a consistent foot-ground contact angle during leg actuation.
- The development of a complete kinematic model, including forward and inverse kinematics, for the proposed mechanism.
- The formulation of a trajectory planning method tailored to the unique geometry and motion of the design.
- Experimental validation of the proposed design, demonstrating improved energy efficiency via the Cost of Transport (C.O.T.) [20] metric compared to a baseline model without the angle-bisecting mechanism.

The remainder of this paper is organized as follows. Section

This work was supported by the National Science and Technology Council (NSTC), Taiwan, under Contracts 113-2221-E-002 -097 -MY3.

The authors are with the Department of Mechanical Engineering, National Taiwan University, Taipei 10617, Taiwan (*corresponding author email: peichunlin@ntu.edu.tw).

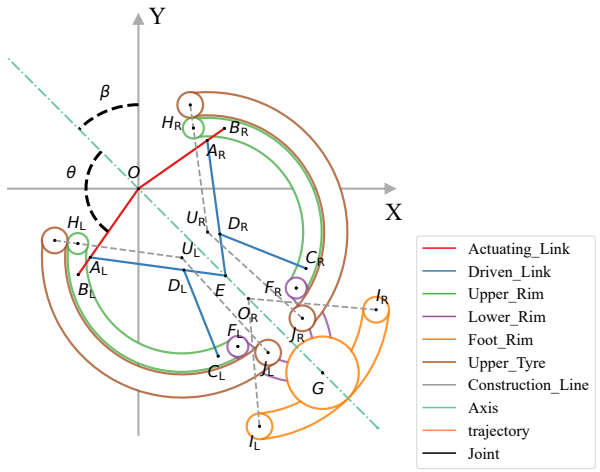

Fig. 2: Configuration of the leg-wheel mechanism. Different segments of the mechanism are highlighted in different colors and labels.

II details the mechanical design of the novel leg-wheel, focusing on the motivation, selection, and implementation of the angle-bisecting mechanism. Section III presents the complete kinematic model and the development of the motion planning framework, from single-leg trajectory generation to quadruped gait coordination. Section IV describes the experimental setup and presents a detailed discussion of the results, including a direct performance comparison with a baseline model and an analysis of the energy-stability trade-off. Finally, Section V concludes the paper and outlines future research directions.

II. Mechanism Design

This section details the mechanical design of the novel leg-wheel, focusing on the core innovation: an integrated angle-bisecting foot mechanism. The design is an evolution of the leg-wheel transformable robot previously presented in [21]. While the base leg linkage provides effective transformation between wheeled and legged modes, it introduces a challenge in maintaining stable foot-ground contact.

A. Design Goals and Requirements

The foundational leg structure, depicted in Fig. 2, utilizes a symmetrical linkage where the left and right side of lower rims (Lower Rim L/R) deploy and retract in concert. A critical consequence of this symmetrical actuation is that the angle of the foot relative to the ground would continuously change without a corrective mechanism. This angular variation can lead to unstable point/edge contact, increasing the risk of slippage and reducing the efficiency of force transmission, particularly on non-flat terrains.

Therefore, the primary design goal was to develop a mechanism that passively and automatically maintains a consistent orientation of the footpad relative to the leg's line of symmetry. This requires a mechanism capable of dynamically calculating and holding the angle bisector of the two lower links, ensuring the Foot Rim remains parallel to the ground during the stance phase, regardless of the leg's deployment angle. This approach embodies the principle of "mechanical intelligence," where a computational task—in this case, angle averaging—is offloaded from the software-based control system and embedded directly into the physical structure of the mechanism. By solving the geometric constraint passively, the design simplifies the control problem, reduces potential software latencies, and enhances the robot's physical responsiveness and robustness without the need for additional sensors or actuators.

B. Possible Mechanisms for the Angle-Bisecting Mechanism

To achieve the design goal, we evaluated several mechanical solutions for implementing an angle-bisecting function. The key selection criteria were structural rigidity, compactness for integration into the distal end of the leg, and reliability under dynamic loading. The following options were considered:

- Linkage Mechanisms: While configurations like parallel four-bar linkages can maintain angular relationships , they are often susceptible to deformation and backlash under the high-impact loads experienced during locomotion. Furthermore, achieving precise angle bisection over a wide range of motion with simple linkages often involves "structural error" inherent to function generation, while mathematically exact solutions like the Peaucellier-Lipkin linkage are typically too complex for this application. Poor transmission angles can also compromise dynamic performance and lead to binding.
- Differential Gear Mechanisms: These can effectively compute the angle average but tend to be complex and bulky, making them unsuitable for the space-constrained foot assembly.
- Cable-Pulley Systems: Although lightweight, these systems are prone to cable stretching and slack, which compromises positional accuracy and long-term reliability.
- Planetary Gear Mechanisms: This approach offers a compact, robust, and highly efficient solution for torque transmission and precise angular control. The inherent properties of a planetary gear train allow it to function as a mechanical averager.

Based on this comparative analysis, a planetary gear mechanism was selected as the most suitable solution due to its superior combination of high rigidity, compact form factor, and dependable performance, which are all critical for a dynamic robotic leg application.

C. Implementation of the Planetary Gear Mechanism

The core of the angle-bisecting mechanism is a custom, two-stage compound planetary gear train, as depicted in Fig. 3. To analyze its kinematics, we first map the components of our design to standard planetary gear terminology. The two lower leg links, 'Lower Rim L' and 'Lower Rim R', serve as the system's inputs, while the 'Foot Rim' is the output. In this two-stage compound design, 'Lower Rim R' functions as the common planet carrier (C) for both stages. 'Lower Rim L' is rigidly connected to the ring gear of the first stage (R_1), and the 'Foot Rim' is connected to the ring gear of the second stage (R_2). Both stages share a common, concentric sun gear shaft

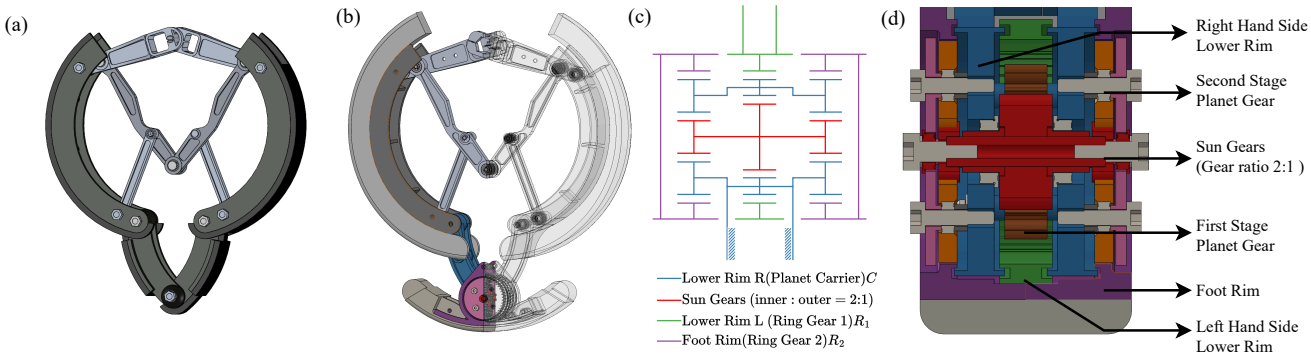

Fig. 3: The CAD illustration of the leg-wheel mechanism: (a): The front view of the original leg-wheel mechanism. (b): cross-section view of the leg-wheel. (c) The kinematic diagram of the planetary gear transmission. (d)The blow-up cross-section view of the planetary gear transmission.

(S), which constrains their sun gears to rotate together $\omega_{S1} = \omega_{S2} = \omega_S$. The kinematic relationship is governed by the Willis Equation, which for any stage relates the angular velocities of the sun (ω_S), ring(ω_r), and carrier(ω_c) in the carrier's reference frame as

$$\frac{\omega_S - \omega_c}{\omega_r - \omega_c} = \frac{Z_r}{Z_s} \tag{1}$$

where Z is the number of teeth. Let ω_L, ω_R and ω_F be the absolute angular velocities of 'Lower Rim L', 'Lower Rim R', and 'Foot Rim', respectively. Applying (1) to Stage 1, where the carrier is 'Lower Rim R' ($\omega_c = \omega_R$) and the ring is 'Lower Rim L' ($\omega_r = \omega_L$) , we can solve for the sun gear's velocity ω_S. Applying (1) again to Stage 2, where the carrier is also 'Lower Rim R' ($\omega_c = \omega_R$) but the ring is the 'Foot Rim' ($\omega_r = \omega_F$), we obtain a second expression for the same sun gear velocity ω_S. By equating these two expressions for ω_S, we derive a direct relationship between the relative velocities of the inputs and the output:

$$\frac{Z_{R1}}{Z_{S1}}(\omega_L - \omega_R) = \frac{Z_{R2}}{Z_{S2}}(\omega_F - \omega_R) \tag{2}$$

This reveals that the final motion is a function of the gear tooth ratios between the two stages. For this mechanism, we specifically designed the gear train such that the ring gears have the same number of teeth ($Z_{R1} = Z_{R2}$) and the first sun gear has twice the teeth of the second ($Z_{S1} = 2Z_{S2}$). Substituting these ratios into the derived kinematic equation simplifies it to the final relationship:

$$(\omega_L - \omega_R) = 2(\omega_F - \omega_R) \tag{3}$$

This result, expressed in relative velocities as

$$\begin{aligned} \omega_{L/R} &= 2\omega_{F/R} \\ \Rightarrow \omega_{F/R} &= \frac{1}{2}\omega_{L/R} \end{aligned} \tag{4}$$

Then integrating the relative velocity with respect to time yields the angular relationship:

$$\theta_{F/R} = \frac{1}{2}\theta_{L/R} + C \tag{5}$$

where C is an integration constant determined by the initial assembly alignment of the gears. By properly setting the initial phase of the gears such that $C = 0$, this proves that the angle of the 'Foot Rim' relative to 'Lower Rim R' is always exactly half the angle of 'Lower Rim L' relative to 'Lower Rim R', thus mechanically enforcing the desired angle-bisecting property. The two-stage design was necessary because achieving this specific 2:1 relative ratio is not feasible with a single-stage planetary gear train while maintaining the required direction of rotation.

D. Fabrication and Materials

The entire foot assembly was fabricated using Fused Deposition Modeling (FDM) with a multi-material additive manufacturing approach (Fig. 4). This method was specifically chosen for its ability to produce the complex internal geometries of the planetary gear system while allowing for the strategic use of advanced engineering-grade filaments.

The primary structural material used for the housing and linkages is eSUN's PAHT-CF, a carbon fiber reinforced high-temperature nylon. This material was selected for its excellent mechanical properties, including high strength, rigidity, and impact resistance, which are critical for withstanding the dynamic loads experienced during locomotion.

For the outer surface of the Foot Rim, which serves as the direct interface with the ground, we utilized eSUN's TPU-LW (Lightweight TPU). This filament offers two key advantages. Firstly, its foaming properties allow us to precisely control the material's hardness and compliance by tuning printing parameters such as temperature and flow rate, enabling the creation of a high-friction, shock-absorbing contact surface. Secondly, PAHT-CF serves as an excellent support material for TPU-LW, allowing us to print complex overhanging structures on the flexible tyre.

This co-printing strategy is crucial as it ensures a superior chemical and mechanical bond between the rigid PAHT-CF structure and the flexible TPU tyre, an outcome difficult to achieve reliably with traditional post-assembly adhesives. The resulting monolithic part not only reduces assembly complexity and minimizes potential points of failure but also guarantees a robust and delamination-resistant interface between the

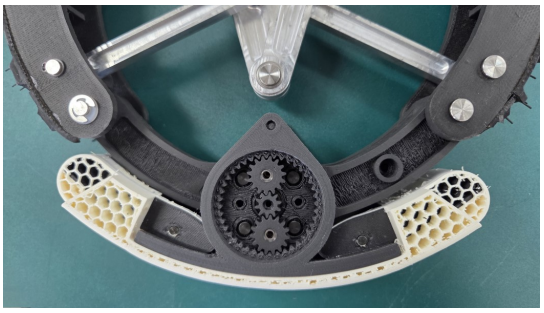

Fig. 4: 3D printed Gear and foot assembly

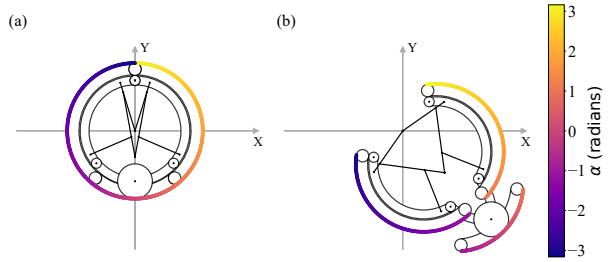

Fig. 5: Definition of the contact angle α for the leg-wheel mechanism: α ranges from -180 deg to 180 deg, increasing positively in the clockwise direction.

main structure and the tyre, enabling a highly compact and durable design.

While this fabrication approach offers significant advantages in creating complex, integrated geometries, it is important to acknowledge its potential limitations for long-term, high-impact applications. The durability of 3D-printed polymer gears, even when reinforced, may be a concern regarding long-term wear and fatigue compared to traditional machined metal or Delrin components. Furthermore, manufacturing tolerances inherent to FDM could introduce backlash into the gear train, potentially affecting the precision of the angle-bisecting function. A comprehensive analysis of the mechanism's long-term reliability under cyclic loading remains a subject for future investigation.

III. Modeling and Motion Planning

To enable precise control and motion planning for the proposed leg-wheel, a comprehensive kinematic model was developed. This chapter details the forward and inverse kinematics of the leg, as well as the high-level trajectory planning model used to define key gait parameters.

A. Forward Kinematics

The forward kinematics model is developed in two stages. First, we define the positions of key structural points on the leg linkage. Second, we establish a parametric model to describe any point on the continuous curve of the foot rim. To achieve this, we first define a local coordinate frame $\{L\}$ for the leg, with its origin at the hip joint O.

1) Kinematics of Structural Joints: The kinematic model for the base 11-linkage leg-wheel mechanism is adapted from a previously presented model in [21]. This revised model has been extended to include additional foot linkages required to fully define the new foot mechanism. Using complex number notation to represent 2D vectors in the leg frame $\{L\}$, the key points $\hat{I}$ and $\hat{J}$ on the foot rim are defined as:

$$\hat{I} = \hat{O}_r + Re^{i\angle GO_rI} \quad ,\angle GO_rI = \quad 40 \text{ deg} \tag{6}$$

$$\hat{J} = \hat{U} + Re^{i(\angle \vec{UH} + \angle HUJ)} \quad ,\angle HUK = \quad 140 \text{ deg} \tag{7}$$

Here, $\hat{O}_r$ and $\hat{U}$ are vectors representing the positions of intermediate joints, and R is a characteristic radius.

2) Parametric Kinematics of the Foot Rim: Since any point on the rim could potentially make contact with the ground, the continuous contact surface is parameterized by a variable α, as illustrated in Fig. 5. The position of any point $\mathrm{P}(\alpha)$ on the rim within the leg frame $\{L\}$ is given by the following piecewise function:

$$\mathrm{P}(\alpha)_{\{L\}} = \begin{cases} \vec{U_R} + R \times \mathrm{rot}(\alpha - \overset{\frown}{FG}) \frac{\vec{U_R J_R}}{|\vec{U_R J_R}|} & ,\alpha > \overset{\frown}{FG} \\ \vec{O_r} + R \times \mathrm{rot}(\alpha) \frac{\vec{O_r G}}{|\vec{O_r G}|} & ,\overset{\frown}{FG} \leq \alpha \leq \overset{\frown}{FG} \\ \vec{U_L} + R \times \mathrm{rot}(\alpha + \overset{\frown}{FG}) \frac{\vec{U_R J_R}}{|\vec{U_R J_R}|} & ,\alpha < -\overset{\frown}{FG} \end{cases} \tag{8}$$

where $\vec{U_L}$, $\vec{U_R}$, and $\vec{O_r}$ represent the center points of the different circular sections of the rim, R is the rim radius, rot represents the rotation matrix to rotate vectors in the counter-clockwise direction , and $\overset{\frown}{FG}$ defines the transition angles between segments. To transform this position from the leg frame $\{L\}$ to the robot's root frame $\{R\}$, a rotation matrix $\mathbf{R}_L^R$ is applied, which depends on the leg's hip angle β:

$$\mathrm{P}_{\{\mathrm{R}\}} = \mathbf{R}_L^R \mathrm{P}_{\{\mathrm{L}\}} = \begin{bmatrix} \cos\beta & -\sin\beta \\ \sin\beta & \cos\beta \end{bmatrix} \mathrm{P}_{\{\mathrm{L}\}} \tag{9}$$

This model allows for the complete description of the leg's workspace and the precise positioning of the foot for ground interaction.

B. Inverse Kinematics

The inverse kinematics problem involves determining the required actuator and hip angles (θ, β) to place a specific point on the foot rim at a desired target coordinate P target in the robot's frame. This requires solving the non-linear equations derived from the forward kinematics model. Due to the complexity of the linkage and the piecewise nature of the foot rim description, an analytical solution is intractable. Therefore, we employ numerical methods, such as iterative Jacobian-based solvers, to find the joint angles that minimize the error between the current foot position and the target position.

C. Leg-Wheel Trajectory Planning

The generation of a single-leg trajectory is divided into two distinct phases: the stance phase, where the foot is in contact with the ground, and the swing phase, where the foot is repositioned for the next step.

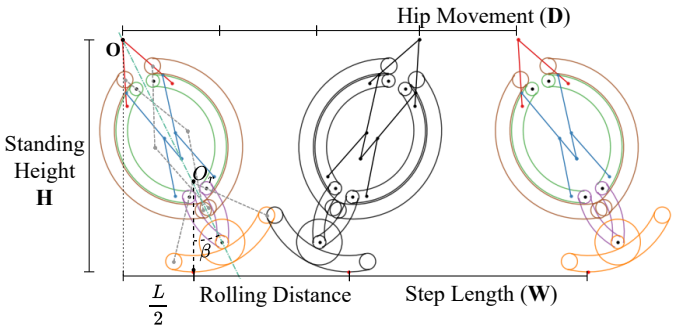

Fig. 6: Parameters for trajectory planning of the leg-wheel mechanism. standing height H: the distance from the hip point to the ground. Step length W: the distance from the lift-off point to the touch-down point.Hip movement D: the hip movement between two steps.

1) Stance Phase Trajectory: During the stance phase, the ideal motion of the foot rim against the ground is pure rolling. A key feature of our design is the angle-bisecting planetary gear mechanism, which ensures that the tangent at the contact point is always parallel to the ground, and thus the contact normal is always perpendicular. This geometric constraint significantly simplifies the control problem. Instead of solving a full two-dimensional inverse kinematics problem for the foot's Cartesian coordinates (x, y), we can reduce it to a one-dimensional problem. By specifying the desired horizontal velocity or displacement of the robot's body, the pure rolling constraint dictates the corresponding vertical position of the foot. This allows for a more direct mapping from the task-space trajectory to the required joint-space commands, improving computational efficiency and robustness.

The simplified model and key parameter description is shown in Fig. 6. These parameters are geometrically related through a set of simplified equations based on the leg deployment angle β and the effective leg length $\overline{OO_r}$, which is a function of the main actuator angle θ:

$$\overline{OO_r} = f(\theta) \tag{10}$$

$$H = R + \overline{OO_r}\cos\beta \tag{11}$$

$$L = 2\overline{OO_r}\sin\beta \tag{12}$$

$$D = \frac{L + 2R\beta}{(n-1)} \tag{13}$$

where n stands for the amount of steps in a gait period, $n = 4$ for walking gait, and $n = 2$ for trotting gait.

$$W = L + D \tag{14}$$

after applying (11) into (14), we could derive relationships between W, H, β:

$$W = \frac{2}{n-1}[n(H-R)\tan\beta + R\beta] \tag{15}$$

This equation is pivotal. For a given set of desired gait parameters, W and H, it can be solved numerically to find the required deployment angle β. Subsequently, the corresponding actuator angle θ is determined by inverting the function

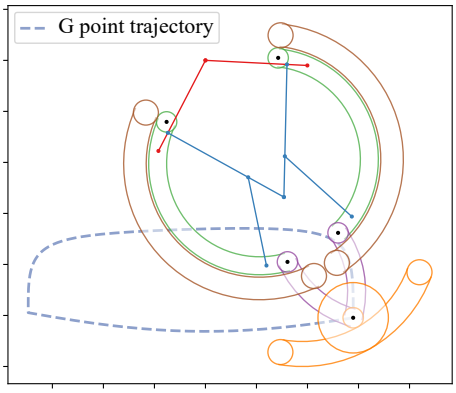

Fig. 7: Trajectory of the point **G** of the leg-wheel mechanism represented in the leg frame.

$\overline{OO_r} = f(\theta)$. This process allows us to calculate the necessary initial and final leg configurations for each step. Once the boundary conditions of the stance phase are defined, the continuous trajectory is generated. By discretizing time, the leg configuration at the next time step,t_{k+1}, can be derived from the current state at t_k and the desired horizontal body velocity, v_x. This dynamic relationship, derived from the pure rolling constraint, is expressed as:

$$v_x(t_{k+1} - t_k) = (H-R)(\sin\beta_k - \sin\beta_{k+1}) + R(\beta_{k+1} - \beta_k) \tag{16}$$

For motions involving a change in standing height, the trajectory generation is decoupled. The vertical positioning is achieved first by adjusting the actuator angle θ. Once the desired height is reached, the pure-rolling-based method is then utilized for subsequent horizontal movement.

2) Swing Phase Trajectory: For the swing phase, the foot is lifted from the ground and propelled forward to the desired touchdown point for the next stance phase. In the absence of ground contact constraints, the trajectory can be optimized for objectives such as obstacle clearance and energy efficiency. For this purpose, the swing phase trajectory is generated using an optimized Bézier curve, following a method established in [22]. Bézier curves are well-suited for this task as they generate a smooth C^2 continuous path, and their shape can be intuitively controlled by adjusting a set of control points. By appropriately defining these points, we can precisely shape the trajectory to ensure sufficient ground clearance while minimizing inertial effects, thereby preparing the leg for a stable and predictable landing.

D. Robot Gait Planning

To achieve stable locomotion, the single-leg trajectories are coordinated across all four legs using a statically stable crawling gait. We employ a footfall sequence of K_{1324} (Leg Front Left(FL) - Rear Right(RR) - Front Right(FR) - Rear Left (RL)), a pattern adapted from prior research on multi-legged robots [23].

The gait timing is governed by a master phase variable,ϕ, which is normalized to a full cycle of $[0, 2]$. Each leg's motion

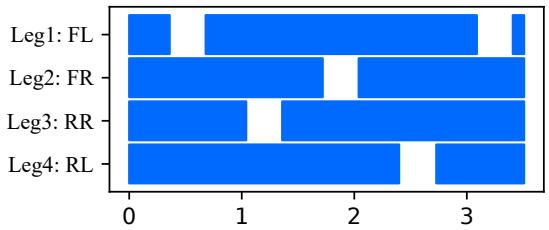

Fig. 8: Statically stable crawling gait used in the experiments, the leg phase diagram shows the K_{1324} footfall pattern, where solid bars indicate the stance phase, and the gaps indicate the swing phase.

TABLE I: Specifications of the Robot

Parameter	Sub-Parameter	Value	Unit
Weight	Body	23	kg
Body Dimension	Length	0.62	m
	Width	0.33	m
	Height	0.17	m
	Wheelbase	0.44	m
Leg-Wheel Dimension	Wheel Radius	0.134	m
	Max Leg Length	0.35	m

consists of a swing phase, defined as $\phi \in [0, 0.5]$, and a subsequent stance phase, defined as $\phi \in (0.5, 2]$. This timing corresponds to a duty factor of 75%, ensuring at least three legs are in contact with the ground at all times.

The trajectory for each leg follows this master phase but with a specific offset. A key feature of our implementation is the introduction of quad-contact support phases between each leg swing, as illustrated in the leg phase diagram in Fig. 8. The phase offsets are specifically timed to create these periods of maximum stability and are set as follows:

$$\begin{aligned} \phi_{\text{FL}} &= \phi && \mod 2 \\ \phi_{\text{FR}} &= (\phi + 1.0) && \mod 2 \\ \phi_{\text{RR}} &= (\phi + 1.5) && \mod 2 \\ \phi_{\text{RL}} &= (\phi + 0.5) && \mod 2 \end{aligned}$$

A significant advantage of the pure rolling motion during the stance phase is the ability to maintain continuous forward body motion even when multiple feet are on the ground. Unlike gaits that require the body to pause while legs are repositioned, our approach allows for periods where all four feet are in ground contact while the robot's body maintains a constant forward velocity. This combines the high stability of a crawl gait with the smooth and efficient progression of rolling locomotion.

IV. EXPERIMENTS AND RESULTS

This chapter presents the experimental validation of the proposed leg-wheel mechanism. We first describe the hardware platform and our multi-stage experimental procedure. This procedure was designed to first broadly map the performance landscape, then identify optimal operating regions, and finally conduct a direct, rigorous comparison between the proposed "New" design and the baseline "OLD" design, focusing on the crucial trade-off between energy efficiency and stability.

A. Experimental Setup

1) Hardware Platform: Experiments were conducted on our custom-built leg-wheel transformable robot, as shown in Fig. 1. Detailed specifications are provided in Table I. The core foot mechanism was fabricated using multi-material 3D printing, which allows for the monolithic integration of its complex internal geometries, ensuring both structural integrity and light weight.

2) Control Group (Baseline Design): To rigorously evaluate the benefits of the proposed angle-bisecting mechanism, a control group was established. This "OLD" baseline design consists of a simplified foot where the foot rim is rigidly fixed to the leg linkage (Fig. 3(a)), lacking any corrective mechanism for maintaining ground contact posture. Both the "NEW" angle-bisecting design and the "OLD" baseline design share identical link proportions and utilize the exact same motion planning and gait coordination frameworks described in Section III. This ensures that any performance variations are strictly attributable to the proposed mechanical innovation.

3) Environment and Experimental Data Collection: All experiments were performed on a flat indoor surface equipped with a VICON motion capture system to ensure consistent and repeatable test conditions. The VICON system was used to accurately track the robot's pose and velocity, while the instantaneous total input power, P, was calculated by monitoring the DC bus voltage and current of the motor drivers.

B. Analysis of the Robot Motion Parameter Landscape

We conducted a comprehensive analysis to understand how different gait parameters affect the performance of the "New" design, using the Cost of Transport (C.O.T.) as the performance metric. The C.O.T. is a widely accepted, dimensionless standard that normalizes energy consumption by the robot's weight and travel distance, allowing for fair comparisons of locomotive efficiency across different robots. Unlike mechanical advantage, which only describes static force transmission ratios, C.O.T. captures the overall dynamic energy efficiency of the system. It is defined as:

$$\text{C.O.T} = \frac{\int P dt}{mgS} = \frac{\int P dt}{mgvT} = \frac{P_{\text{avg}}}{mgv} \tag{17}$$

Where P and P_{avg} stand for instantaneous and average power, m is the robot mass, g is the gravity constant, and v is the robot speed.

The experimental data was rendered as a series of C.O.T. contour plots, as shown in Fig. 9. Each plot illustrates the C.O.T. across a two-dimensional parameter space defined by the robot's standing height (H) and the gait ratio ($\lambda = W/H$) for a constant forward velocity.

These plots reveal a distinct "valley" of low C.O.T. for each velocity, representing the most energy-efficient operating region. A key finding is that the location and shape of this optimal region are velocity-dependent. At lower speeds (e.g., V=0.05 m/s), the most efficient gaits are characterized by a lower standing height (H $\approx$ 22$\sim$24 cm) and a moderate gait ratio ($\lambda \approx$ 1.0$\sim$1.2). As the forward velocity increases, the

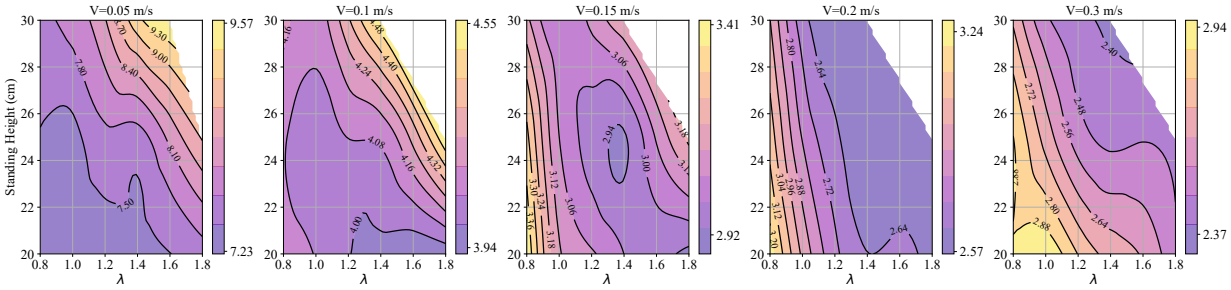

Fig. 9: Contour plots of C.O.T. as a function of standing height (H) and Gait Ratio (λ) for five different velocities of the robot, the experiment was test using 5 different velocities, 3 different standing height, and 9 different gait ratio

optimal region tends to shift towards slightly higher standing heights and larger gait aspect ratios. For instance, at V=0.3 m/s, the lowest C.O.T. is achieved at a standing height of H $\approx$ 24$\sim$26 cm and a gait ratio of $\lambda \approx$ 1.4$\sim$1.6.

This analysis demonstrates that the most energy-efficient gait is not defined by a single parameter but by an optimal combination of standing height and step length that varies dynamically with the robot's speed. This provides a valuable guideline for developing adaptive gait controllers that can optimize for energy efficiency in real time.

C. Locomotion Performance of the Robot with and without new angle-bisecting mechanism

To directly compare the performance of the proposed "New" design against the baseline "OLD" design, a series of experiments were conducted under three distinct gait conditions, as detailed in Table II. These conditions were selected to represent slow, medium, and fast locomotion speeds, with gait parameters chosen from the optimal performance regions identified in our earlier tests.

The results, summarized in Table III and visualized in Fig. 10, reveal a speed-dependent performance trade-off. At the lowest tested speed (Exp. 139, v=0.05 m/s), the "New" design's C.O.T. was marginally higher, as the parasitic friction from the planetary gear system represented a larger portion of the total energy consumption at this low power level.

However, as speed increased, the stability benefits of the mechanism became dominant. At the fastest speed (Exp. 141, v=0.15 m/s), the "New" design achieved a statistically significant 16.2% reduction in C.O.T. ($p < 0.001$). As shown in Fig. 10, this is because the stable, pure rolling motion of the new design avoids the large, frequent power spikes characteristic of the "OLD" design, which suffered from instability and foot slippage. Concurrently, the new design enhanced locomotion stability across all conditions, with a notable 28.6% reduction in pitch fluctuation (σ_{pitch}) in Exp. 140 (v=0.10 m/s), which was also highly statistically significant ($p < 0.001$).

These results validate that while a minor energy trade-off exists at very low speeds, the proposed angle-bisecting foot mechanism provides a significant and robust improvement in locomotion stability, which translates to superior energy efficiency at practical operating speeds.

TABLE II: Robot motion parameters for experimental validation

Exp	h (cm)	l (cm)	v (m/s)	λ
139	23.0	23.0	0.05	1.00
140	24.0	26.4	0.10	1.10
141	24.5	33.1	0.15	1.35

TABLE III: Comparison between new and old gaits

Exp	Type	Power (W)	COT	σ_{pitch}(deg)
139	New	90.91 $\pm$ 0.02	8.06$\pm$0.00	1.27$\pm$0.02
139	OLD	83.80 $\pm$ 0.59	7.43$\pm$0.05	1.29$\pm$0.01
140	New	96.41 $\pm$ 0.24	4.27$\pm$0.01	0.87$\pm$0.01
140	OLD	97.52 $\pm$ 0.37	4.32$\pm$0.02	1.20$\pm$0.00
141	New	96.64 $\pm$ 0.16	2.86$\pm$0.03	0.76$\pm$0.01
141	OLD	115.29 $\pm$ 0.35	3.41$\pm$0.01	0.97$\pm$0.02

V. CONCLUSION AND FUTURE WORK

This paper presents the design, modeling, and experimental validation of a novel leg-wheel mechanism featuring an integrated, passive angle-bisecting foot mechanism. The core of the design is a two-stage planetary gear system that mechanically ensures a consistent foot-ground contact angle, addressing a key limitation in the leg-wheel robots with symmetrical legs. We developed a complete kinematic model and a hierarchical motion planning framework that leverages the pure rolling motion enabled by this mechanism.

The effectiveness of the proposed design was validated through a comprehensive set of hardware experiments. A direct comparison with a baseline design (lacking the angle-bisecting mechanism) demonstrated that our new mechanism achieves a significant improvement in both energy efficiency and stability, with up to a 16.2% reduction in the C.O.T. and a 28.6% reduction in pitch oscillation under tested conditions. Furthermore, our analysis of the performance landscape revealed a critical trade-off between energy efficiency and locomotion stability, governed by the gait aspect ratio ($\lambda = W/H$). This provides a valuable guideline for selecting optimal gait parameters based on specific task requirements.

For future work, we plan to extend this research in several directions. First, we will conduct a more extensive set of experiments on varied and uneven terrains to fully characterize the benefits of the passive terrain adaptability afforded by the foot mechanism. Second, we will leverage the presented kinematic model to develop more dynamic gaits, such as trotting and leaping [24], to enhance the robot's agility and speed. Finally,

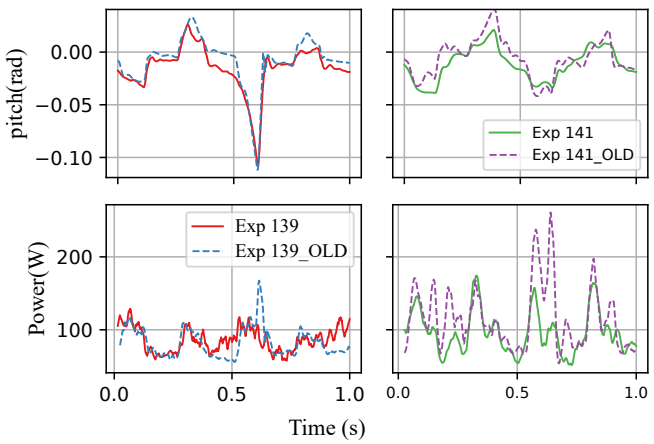

Fig. 10: Comparison of pitch stability and power consumption in one gait-sequence for the proposed (solid red/green lines) and baseline (dashed blue/purple lines) mechanisms under two different gait conditions (Exp. 139 and Exp. 141).

future work will involve integrating established methods for force and body estimation [25], [26] and motion modeling [27]. This will enable the implementation of closed-loop force control strategies, further improving the robot's robustness and adaptability in challenging, unstructured environments.

REFERENCES

[1] G. Bledt, M. Powell, B. Katz, J. Di Carlo, P. Wensing, and S. Kim, "Mit cheetah 3: Design and control of a robust, dynamic quadruped robot," in *2018 IEEE/RSJ International Conference on Intelligent Robots and Systems (IROS)*, 2018, pp. 2245–2252.

[2] E. Guizzo, "By leaps and bounds: An exclusive look at how boston dynamics is redefining robot agility," *IEEE Spectrum*, vol. 56, no. 12, pp. 34–39, 2019.

[3] C. Semini, V. Barasuol, J. Goldsmith, M. Frigerio, M. Focchi, Y. Gao, and D. Caldwell, "Design of the hydraulically actuated, torque-controlled quadruped robot hyq2max," *IEEE/ASME Transactions on Mechatronics*, vol. 22, no. 2, pp. 635–646, 2017.

[4] M. Bjelonic, P. Sankar, C. Bellicoso, H. Vallery, and M. Hutter, "Rolling in the deep – hybrid locomotion for wheeled-legged robots using online trajectory optimization," *IEEE Robotics and Automation Letters*, vol. 5, no. 2, pp. 3626–3633, 2020.

[5] Q. Zhou, S. Yang, X. Jiang, D. Zhang, W. Chi, K. Chen, S. Zhang, J. Li, J. Zhang, R. Wang, J. Li, Y. Zhang, H. Wang, S. Wang, L. Xiang, Y. Zheng, and Z. Zhang, "Max: A wheeled-legged quadruped robot for multimodal agile locomotion," *IEEE Transactions on Automation Science and Engineering*, vol. 21, no. 4, pp. 7562–7582, 2024.

[6] C. Sun, G. Yang, S. Yao, Q. Liu, J. Wang, and X. Xiao, "Rhex-t3: A transformable hexapod robot with ladder climbing function," *IEEE/ASME Transactions on Mechatronics*, vol. 28, no. 4, pp. 1939–1947, 2023.

[7] Z. Ju, K. Wei, and Y. Xu, "From concept to field trials: Design, analysis, and evaluation of a novel quadruped robot with deformable wheel–foot structure," *IEEE Transactions on Robotics*, vol. 41, pp. 3143–3161, 2025.

[8] N. Kau, A. Schultz, N. Ferrante, and P. Slade, "Stanford doggo: An open-source, quasi-direct-drive quadruped," in *2019 International Conference on Robotics and Automation (ICRA)*, 2019, pp. 6309–6315.

[9] L. Bai, J. Guan, X. Chen, J. Hou, and W. Duan, "An optional passive/active transformable wheel-legged mobility concept for search and rescue robots," *Robotics and Autonomous Systems*, vol. 107, pp. 145–155, 2018. [Online]. Available: https://www.sciencedirect.com/science/article/pii/S0921889018301891

[10] K. Nasonov, D. Ivolga, I. Borisov, and S. Kolyubin, "Computational design of closed-chain linkages: Hopping robot driven by morphological computation," in *2023 IEEE International Conference on Robotics and Automation (ICRA)*, 2023, pp. 7419–7425.

[11] S. Feng, Y. Gu, W. Guo, Y. Guo, F. Wan, J. Pan, and C. Song, "An overconstrained robotic leg with coaxial quasi-direct drives for omni-directional ground mobility," in *2021 IEEE International Conference on Robotics and Automation (ICRA)*, 2021, pp. 11 477–11 484.

[12] W. Bosworth, S. Kim, and N. Hogan, "The mit super mini cheetah: A small, low-cost quadrupedal robot for dynamic locomotion," in *2015 IEEE International Symposium on Safety, Security, and Rescue Robotics (SSRR)*, 2015, pp. 1–8.

[13] F. Chen, W. Tao, and D. Aukes, "Development of a dynamic quadruped with tunable, compliant legs," in *2023 IEEE/RSJ International Conference on Intelligent Robots and Systems (IROS)*, 2023, pp. 495–502.

[14] W. Chen, H. Lin, Y. Lin, and P. Lin, "Turboquad: A novel leg–wheel transformable robot with smooth and fast behavioral transitions," *IEEE Transactions on Robotics*, vol. 33, no. 5, pp. 1025–1040, 2017.

[15] S. Chen, K. Huang, W. Chen, S. Shen, C. Li, and P. Lin, "Quattroped: A leg–wheel transformable robot," *IEEE/ASME Transactions on Mechatronics*, vol. 19, no. 2, pp. 730–742, 2014.

[16] Y. Lai, W. Yu, and P. Lin, "Stair climbing of a transformable robot using varying leg-wheel contact points," in *2025 IEEE International Conference on Robotics and Automation (ICRA)*, 2025, pp. 7675–7681.

[17] S. Abad, N. Sornkarn, and T. Nanayakkara, "The role of morphological computation of the goat hoof in slip reduction," in *2016 IEEE/RSJ International Conference on Intelligent Robots and Systems (IROS)*, 2016, pp. 5599–5605.

[18] A. Ranjan, F. Angelini, T. Nanayakkara, and M. Garabini, "Design guidelines for bioinspired adaptive foot for stable interaction with the environment," *IEEE/ASME Transactions on Mechatronics*, vol. 29, no. 2, pp. 843–855, 2024.

[19] M. Catalano, M. Pollayil, G. Grioli, G. Valsecchi, H. Kolvenbach, M. Hutter, A. Bicchi, and M. Garabini, "Adaptive feet for quadrupedal walkers," *IEEE Transactions on Robotics*, vol. 38, no. 1, pp. 302–316, 2022.

[20] S. Seok, A. Wang, M. Chuah, D. Hyun, J. Lee, D. Otten, J. Lang, and S. Kim, "Design principles for energy-efficient legged locomotion and implementation on the mit cheetah robot," *IEEE/ASME Transactions on Mechatronics*, vol. 20, no. 3, pp. 1117–1129, 2015.

[21] H. Chen, T. Wang, K. Ho, C. Ko, P. Lin, and P. Lin, "Development of a novel leg-wheel module with fast transformation and leaping capability," *Mechanism and Machine Theory*, vol. 163, p. 104348, 2021. [Online]. Available: https://www.sciencedirect.com/science/article/pii/S0094114X21001063

[22] K. Lu, I. Chang, W. Yu, and P. Lin, "Trajectory optimization strategy that considers body tip-over stability, limb dynamics, and motion continuity in legged robots," in *2024 IEEE International Conference on Robotics and Automation (ICRA)*, 2024, pp. 5773–5779.

[23] Z. Ju, K. Wei, L. Jin, and Y. Xu, "Investigating stability outcomes across diverse gait patterns in quadruped robots: A comparative analysis," *IEEE Robotics and Automation Letters*, vol. 9, no. 1, pp. 795–802, 2024.

[24] Z. Chen, W. Yu, and P. Lin, "Fast wheeled driving to legged leaping onto a step in a leg-wheel transformable robot," in *2024 IEEE International Conference on Robotics and Automation (ICRA)*, 2024, pp. 11 342–11 348.

[25] Y. Shen, W. Yu, and P. Lin, "Contact force estimation for a leg-wheel transformable robot with varying contact points," in *2025 IEEE International Conference on Robotics and Automation (ICRA)*, 2025, pp. 684–690.

[26] P. Huang, I. Chang, W. Yu, and P. Lin, "Body velocity estimation in a leg–wheel transformable robot without a priori knowledge of leg–wheel ground contacts," in *2024 IEEE International Conference on Robotics and Automation (ICRA)*, 2024, pp. 11 349–11 355.

[27] W. Lu and P. Lin, "The generalized spring-loaded inverted pendulum model for analysis of various planar reduced-order models and for optimal robot leg design," *Bioinspiration & Biomimetics*, vol. 19, no. 2, p. 026017, feb 2024.